

# Modeling dynamics and control of type-3 DFIG wind turbines: Stability, Q Droop function, control limits and extreme scenarios simulation



Sameh A. Eisa

Department of Mechanical and Aerospace Engineering, University of California, Irvine, CA, USA

## ARTICLE INFO

### Keywords:

Wind turbine  
Mathematical model  
Dynamic behavior  
Small-signal stability  
Wind turbine control system  
Q Droop  
Control limits

## ABSTRACT

In this paper, a type-3 DFIG wind turbine is considered for a time domain dynamical study and mathematical modeling. The paper provides a full differential equations based model that is implementable by stiff solvers, such as Matlab ODE15s. The proposed model is validated vs. real measured data. The paper focuses and investigates further the so-called Q Droop function integrated with the wind turbine control system. Even with promising experimental results presented by General Electric studies, this function has rarely been studied throughout the literature. The paper emphasizes the effect of adding the Q Droop function to the reactive power control, and how this affects the whole dynamics in the system. We provide stability and control limits analysis for the system with and without the Q Droop function. Our results supported by simulations suggest the importance of the Q Droop function for stabilizing the system during sudden changes in wind speed, terminal voltage, or a severe drop in impedance. The paper also shows that the system has attraction limits that exceed the control limits suggested by General Electric and others. This can lead to either relaxing/changing the limiters or re-evaluate the state of the art modeling literature.

## 1. Introduction

The generation of renewable energies is increasing rapidly when compared to fossil fuels. According to [1], wind is the fastest growing renewable energy source. In the last two decades, modeling the control components of Wind Turbine Generators (WTGs) and their dynamics has been a rapidly growing area of research. As found in [2], type-3 WTGs are more efficient in extracting power than other types. The review [3] has a detailed study of the Coefficients of Performance ( $C_p$ ) for type-3 and showed that  $C_p$  can go up to a 0.4-0.5 efficiency of extraction. Most of the studies in the literature, such as, General Electric's (GE) studies [4,5] and Electric Power Institute's study [6], suggested Doubly Fed Asynchronous/Induction Generator (DFAG/DFIG) technology for WTGs. Therefore, we consider the type-3 DFAG/DFIG in our paper.

In the literature, there are many sources and studies, mostly in transfer functions (frequency) domain for type-3 WTGs DFIG-based models. Studies such as, but not limited to [4,7,8] explain the modeling aspect in greater detail, while studies such as, but not limited to [9–12] provide partial modeling focused on some parts of the WTG dynamics. The paper [13] studied small-signal stability, showed that as the impedance drops the system loses stability, and performed eigenvalue analysis, all in transfer function domain. Fewer studies analyzed the

model in time domain. However, having the model in time domain is necessary for stronger nonlinear studies. The papers [14–17] introduced some differential equations models while performing their analysis. Both [14,15] performed parameter sensitivity analysis, while [16] studied stability and bifurcation. Also, Miller et al. [18] summarized some of the important results the GE team presented in [4,5]. The topic of [17] is what we are extending in this paper. We are extending the modeling part, simulation results, and adding an entire section of data validation.

### Motivation and objectives of this paper:

- 1) Modeling efforts in time domain for the WTG system, as discussed in the introduction by detail, are scarce. In our previous publications [15–17,19,20] the WTG model was only partially introduced, however, not generalized to include the complex/entire scale of all controls included in major academic resources, such as [13], or manufacturer reports, such as [4,5]. Also, our recent mathematical paper [21], meant to explore the pure mathematical properties (convergence and uniqueness of solutions) for a possible differential equations model to WTGs, laying the ground for a possible comprehensive modeling work that benefit the power systems and/or wind control communities. In this regard, the reader may refer the

E-mail addresses: [seisa@uci.edu](mailto:seisa@uci.edu), [sameheisa235@hotmail.com](mailto:sameheisa235@hotmail.com).

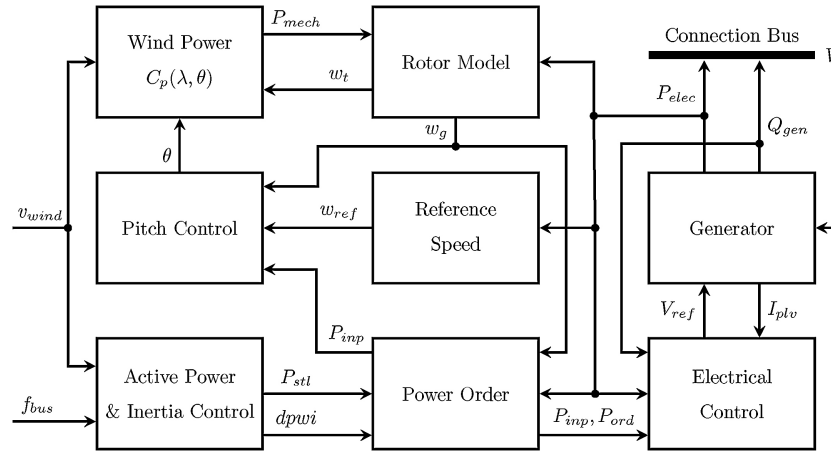


Fig. 1. Connectivity of the model's components.

PhD dissertation [22] for more details. In this paper, we built a full model to the WTG complex control system that is implementable by Matlab ODE15s and other stiff differential equations solvers. Our model then is validated vs. real measured data and [13]. Section 2 of this paper covers this point.

- 2) Throughout the literature (based on our up to date research), we found sparse and rare academic analysis/discussion for the so-called Q Droop function, suggested by GE [5]. While the concept of the Q Droop function has been widely used in the major commercial tools for the second generation generic models for wind and PV plants, it has always been considered in a feedback platform that usually is not clearly explained or analyzed. GE in [5], extended the brief discussion about Q Droop function, and provided new information (compared to [4]) that this function can be also a “constant” and that the gain parameter of the feedback can be tuned/changed. Also, they mentioned that this function can help enhancing the reactive power control performance, all these claims without any documented analysis or further investigations. Note that such documentation has to exist because the state of the art now is to study the WTG as a member in a compound of WTGs, while all of them are interacting with each other. This has been shown to allow WTGs to exploit the available resources in a better way (see [23]). In this paper, we investigate every aspect of the Q Droop function and its effect on the reactive power control and the entire system performance, especially in extreme cases, such as sudden change in wind, voltage or impedance. Section 3 of this paper covers this point.
- 3) In [5], there are limiters (control limits) on the different control blocks (including the integrators of the reactive power control) and some derivatives of the mechanical state variables. However, no discussion was provided for how the imposed control limits on the integrators, state variables, and derivatives would behave in extreme scenarios or even local disturbances. Simulations and tests for the control limits need to be conducted. This can lead to a better utilization of the control limits and the simulators, as one can relax or tighten the limits based on better understanding of such limiters. Section 4 of this paper covers this point.

## 2. The mathematical model

In this section, we build a full time domain mathematical model that can be used by stiff numerical solvers of differential equations (such as ODE15s solve in Matlab). This should allow for deeper and better control studies since the WTG system is highly nonlinear. Also, having the system in time domain allows for non-autonomous simulations that are more practical to present the different scenarios. In order to do that, we explain the control blocks and translate them to differential equations and provide parameter values,  $C_p$  coefficients values, and limiters

values (control limits). Then we provide a solution to the algebraic equation (the network equation), which results in a system of differential equations instead of a system of differential-algebraic equations, allowing for simpler implementation within numerical solvers. The proposed DFIG-based model includes the Q Droop function and includes most of the controls involved in the WTGs system. Lastly, we compare our model with some other models and validate it vs. real time measured data from a WTG.

In our study, the main citations referenced while building the model were [4,5,13,15–17]. In [4], the block diagrams cover the wind power extraction model, rotor model, pitch control, and reactive power control in both the cases power factor and supervisory voltage were provided. In [5],  $C_p$  curves are discussed in more detail and two optional control blocks are added (active power and inertia controls). The GE team in [5] included the Q Droop function. The paper [13], built their model citing [8] and GE studies. The stability of the system was studied in [16], concluding that there is a Hopf bifurcation for small values of the reactance X, which matches and better describes what [13] concluded. We will use the case of a sudden drop in the reactance X as an extreme scenario based on what both [13,16] concluded.

### 2.1. The block diagrams and state variables

We summarized the model blocks and the dynamics between them in Fig. 1, as it shows the primary components of the model as explained in [4,5,13,15]. Units are Per Unit (pu) except for the pitch which is in degrees.

**The wind power model:** The power extracted by the turbine is the power in the air-stream multiplied by  $C_p$ . As mentioned in [5],  $C_p(\lambda, \theta) = \sum_{i=0}^4 \sum_{j=0}^4 \alpha_{i,j} \theta^i \lambda^j$  where the tip ratio is  $\lambda = \frac{K_b w_t}{v_{wind}}$ ,  $\theta$  is the pitch angle, and  $K_b$  is a constant. Fig. 2 shows the  $C_p$  function for some fixed values of  $\theta$ . In the case  $v_{wind} > 11.4$  m/s,  $\theta$  will be in action,

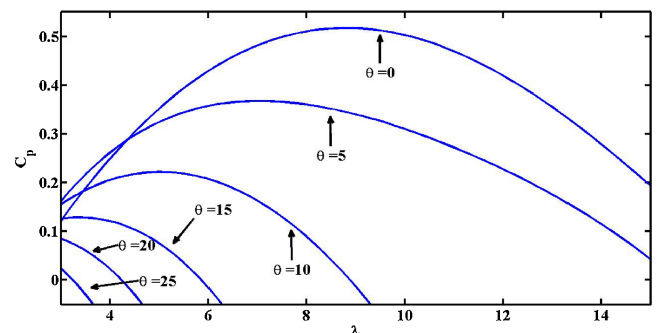


Fig. 2.  $C_p$  curves for some fixed values of  $\theta$ .

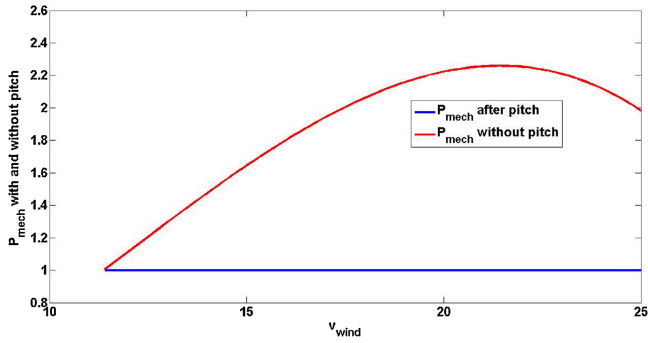


Fig. 3.  $P_{mech}$  with the pitch angle set to zero and the pitch angle in action.

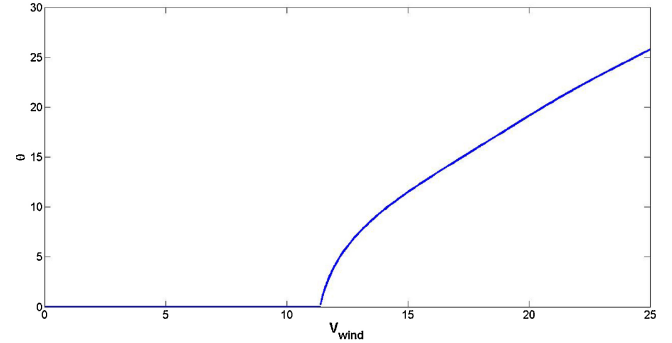


Fig. 6. Pitch angle vs. wind speed.

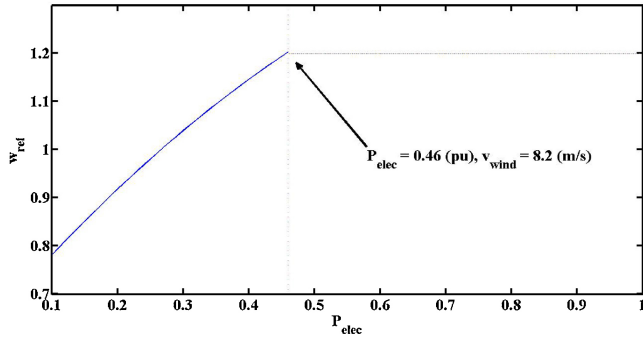


Fig. 4. The reference speed function as a quadratic before  $v_{wind} = 8.2$  m/s and constant after that.

otherwise it is 0. Fig. 3 shows  $P_{mech}$  with the pitch angle set to zero and the pitch angle in action.

**Rotor model and reference speed:** One mass model, as in [24], or two mass model, as in this paper and [4,5,13] can be considered to model the shaft speed and its control. The shaft speed is controlled by a reference speed given by  $w_{ref} = -0.75P_{elec}^2 + 1.59P_{elec} + 0.63$ .  $w_{ref}$  is set to 1.2 (pu) in the case of  $v_{wind} > 8.2$  m/s. Fig. 4 shows the reference speed function. Eqs. (1)–(3) represent the two mass model.  $w_t$ ,  $w_g$  represent the turbine and generator speeds respectively, after adding  $w_0$ . The generator speed is  $w = w_g + w_0$  and the turbine speed is

$w_{rotor} = w_t + w_0$ . Fig. 5 shows the rotor model block diagram.

**Pitch control and compensation:** The pitch angle affects the efficiency of power being extracted from the air. It also keeps the WTG producing the rated power for different wind speeds. Fig. 6 shows the pitch angle steady state vs. wind speeds up to  $v_{wind} = 25$  m/s. Fig. 7 shows the block diagram of the pitch control.  $f_1$  and  $f_2$  are the integrals of  $w_{generator} - w_{ref}$  and  $P_{inp} - P_{stl}$  respectively.

**The power order:** The power order is mainly dependent on the difference between the shaft speed and the reference speed, as well as the shaft speed itself. According to [5], a state variable  $w_{sho}$  is effective during the dynamics as it washes out (reduce the effect) the difference between the output of the active power control and the power order (see Fig. 8). The power order calculation can be modified because of this state variable if the active power and/or inertia controls are activated.

**Reactive power control:** This block feeds reactive power command to the generator and controls the reactive power. This control can use a power factor or supervisory voltage modes. The power factor angle  $PFA$  can be designed as needed. In our study, we assume it as a small constant, so we get a small reactive power compared to the active power. Eq. (11) shows how to generate the reference voltage after having the reactive power command  $Q_{cmd} = \tan(PFA)P_{1elec}$ , where  $P_{1elec}$  is a filtered version of  $P_{elec}$  and they are equivalent in the steady state. Eq. (20) shows the reactive voltage command  $E_{qcmd}$  that goes to the generator. Fig. 9 shows this control. At steady state  $P_{1elec} = P_{elec}$  and

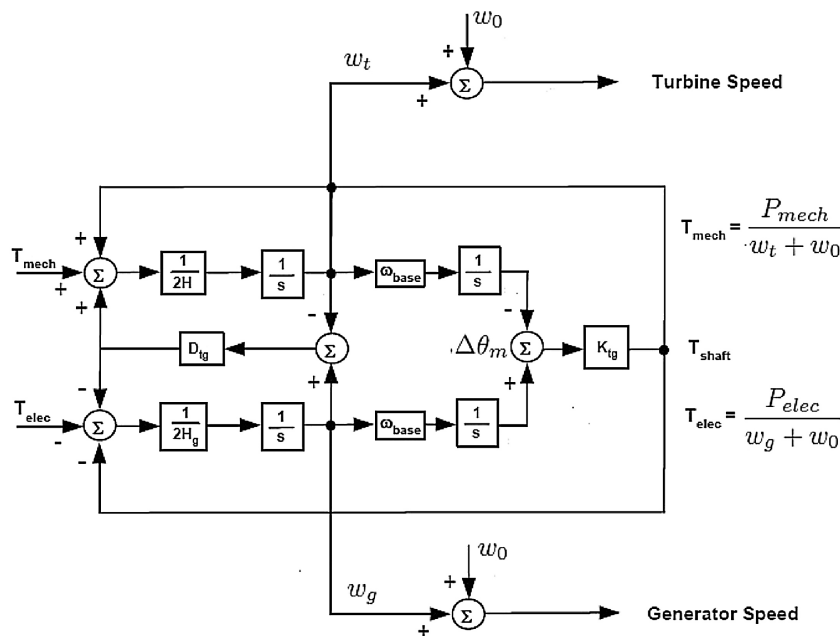


Fig. 5. Rotor model block diagram.

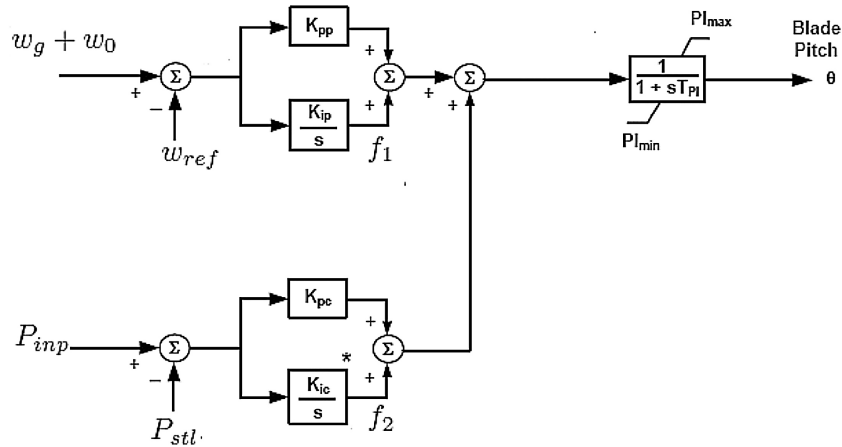


Fig. 7. Pitch control block diagram.

$Q_{cmd} = Q_{gen}, Q_{droop}, V_{1reg}, Q_{wvl}, Q_{wvu}$ , and  $Q_{ord}$  are the state variables in the reactive power control in the case of supervisory voltage (see Fig. 9). All of the state variables except  $Q_{ord}$  represent a transfer function stage.  $V_{1reg}$  is a filtered version of  $V_{ref}$  after passing the  $T_r$  transfer function.  $Q_{wvl}$  and  $Q_{wvu}$  are the output of the transfer functions  $K_{iv}$  and  $T_v$  respectively. Both  $Q_{wvl}$  and  $Q_{wvu}$  combined lead to  $Q_{wv}$ . The output of the transfer function  $T_c$  is the output of the whole control  $Q_{ord}$ .  $Q_{droop}$  can be activated and subtracted from  $V_{1reg}$  after the  $T_r$  transfer function.

**Q Droop function:** Even though the Q Droop function is not a control block, we prefer introducing it in this section as it is an important part of this paper and this model. As shown in Fig. 9, the Q Droop function is only part of the model if the upper branch (supervisory voltage case) of the reactive power control is activated. Q Droop function's dynamic is described in Eq. (12), while the effect of this dynamic appears in the term  $V_{qd} = K_{qd}Q_{droop}$  (see Fig. 9) in Eqs. (14)–(15) to build  $Q_{ord}$  in Eq. (12). The function is put in action simply by setting the gain  $K_{qd} > 0$ . This slow acting function is supposed to reduce the effective reference voltage as reactive power changes. This should improve coordination between multiple integral controllers

regulating the same point in the system as claimed by [5]. The input  $Q_{inpt}$  can be a specified constant or a proportion of the system's reactive power  $Q_{gen}$ . The next section will handle the analysis of adding this function to the dynamics (as a constant or a proportion of the system's reactive power).

**Active power and inertia controls:** These two controls are not activated by default. The main reason for these two controls to exist is to provide changes to the power order the WTG produces based on bus frequency changes (see Fig. 8). The two controls try to provide more power in the case of lower than normal bus frequency (reference frequency) and vice versa. The active power control performs this by setting up the maximum rated power and cutting out, if needed, the available power the WTG has extracted from the air. The inertia control performs the same function, but by providing extra power from the rotor inertia. GE has suggested the use of inertia control, but as mentioned in [5], most current WTGs have yet to implement this.  $P_{avf}$ ,  $f_{ltdfwi}$ , and  $dpwi$  are the state variables of the active power control and the inertia control.  $P_{avf}$  is a filtered version of the available power  $P_{avl}$  that is the input of the active power control. The available power is a

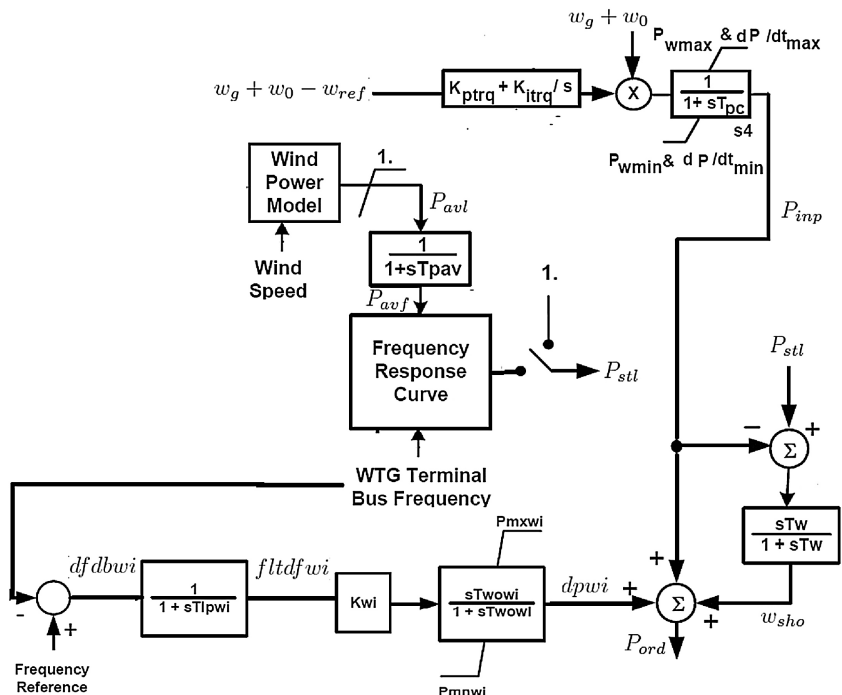


Fig. 8. Block diagrams of power order and optional active and inertia controls.

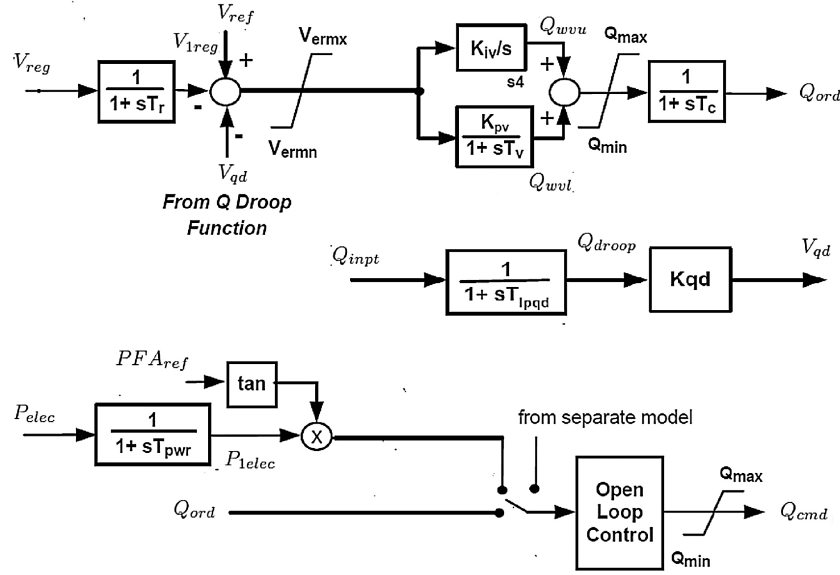


Fig. 9. Reactive power control block diagram.

high proportion of the extracted power, controlled by the frequency curve that depends on design (for example, see pp. 45 in [5]).  $f_{tdfwi}$  is a filtered version of the reference frequency.  $dpwi$  modifies the power order only during the dynamics stage, but approaches zero as we reach the steady state.

**DFIG generator:** The model has two branches that feed the generator, the reactive and the active branches. Eqs. (21)–(22) show how the active current  $I_{plv}$  and the reactive voltage  $E_q$  behave. The network equation provides an algebraic constraint that relates the terminal voltage to the dynamics based on the infinite-bus model of the grid to which the single wind turbine is connected, as in [13], also see Fig. 10. This algebraic constraint is given by Eq. (23). In this equation,  $V$  represents the terminal voltage as a magnitude. In the whole model, as shown in [13], the electric power delivered to the grid is given by  $P_{elec} = VI_{plv}$  and  $Q_{gen} = \frac{V(E_q - V)}{X_{eq}}$ . These formulas are true if the stator resistance is neglected, as introduced in [13].  $E_{qcmd}$ ,  $E_q$ , and  $I_{plv}$  are the generator state variables. Fig. 11 shows the block diagram of the generator variables.

## 2.2. Differential equations, parameters, and control limits

Group 1: Two-mass rotor.

$$\frac{dw_g}{dt} = \frac{1}{2H_g} \left[ -\frac{P_{elec}}{w_g + w_0} - D_{tg}(w_g - w_t) - K_{tg}\Delta\theta_m \right]. \quad (1)$$

$$\frac{dw_t}{dt} = \frac{1}{2H} \left[ \frac{P_{mech}}{w_t + w_0} + D_{tg}(w_g - w_t) + K_{tg}\Delta\theta_m \right]. \quad (2)$$

$$\frac{d(\Delta\theta_m)}{dt} = w_{base}(w_g - w_t). \quad (3)$$

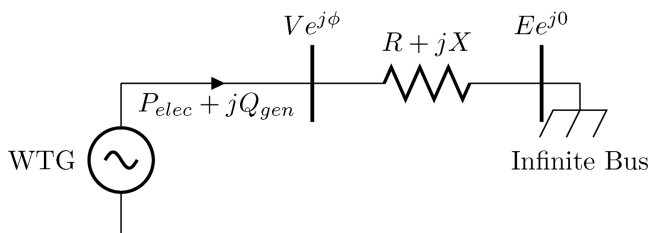


Fig. 10. Single-Machine Infinite-Bus test system.

A one-mass model can be used to simplify the two-mass model in group 1. This has been discussed in [5]. This one-mass differential equation was introduced in [14]. The following equation represents the one mass model:

$$\frac{dw}{dt} = \frac{1}{Hw_{base}} [P_{mech} - P_{elec}].$$

Regardless of whether a two-mass model is used (as in this paper) or one-mass model, we use the following relations:

$$P_{mech} = \frac{1}{2} C_p(\lambda, \theta) \rho A_r v_{wind}^3 = \frac{1}{2} \left( \sum_{i=0}^4 \sum_{j=0}^4 \alpha_{i,j} \theta^i \lambda^j \right) \rho A_r v_{wind}^3$$

and,

$$P_{elec} = VI_{plv}.$$

Group 2: Pitch control.

$$\frac{df_1}{dt} = w_g + w_0 - w_{ref}. \quad (4)$$

$$\frac{df_2}{dt} = P_{inp} - P_{stl}. \quad (5)$$

$$\frac{d\theta}{dt} = \frac{1}{T_p} [K_{pp}(w_g + w_0 - w_{ref}) + K_{ip}f_1 + K_{pc}(P_{inp} - P_{stl}) + K_{ic}f_2 - \theta]. \quad (6)$$

Group 3: Reference speed.

$$\frac{dw_{ref}}{dt} = \frac{1}{60} [-0.75P_{elec}^2 + 1.59P_{elec} + 0.63 - w_{ref}]. \quad (7)$$

Group 4: Power order.

$$\frac{dP_{inp}}{dt} = \frac{1}{T_{pc}} [(w_g + w_0)(K_{ptrq}(w_g + w_0 - w_{ref}) + K_{itrq}f_1) - P_{inp}]. \quad (8)$$

$$\frac{dw_{sho}}{dt} = \frac{dP_{stl}}{dt} - \frac{dP_{inp}}{dt} - \frac{1}{T_w} w_{sho}. \quad (9)$$

$$P_{ord} = \begin{cases} P_{inp} & \text{Group 7 (deactivated)} \\ P_{inp} + w_{sho} & \text{Only active Power control (activated)} \\ P_{inp} + dpwi & \text{Only inertia control (activated)} \\ P_{inp} + w_{sho} + dpwi & \text{Group 7 (activated)} \end{cases}$$

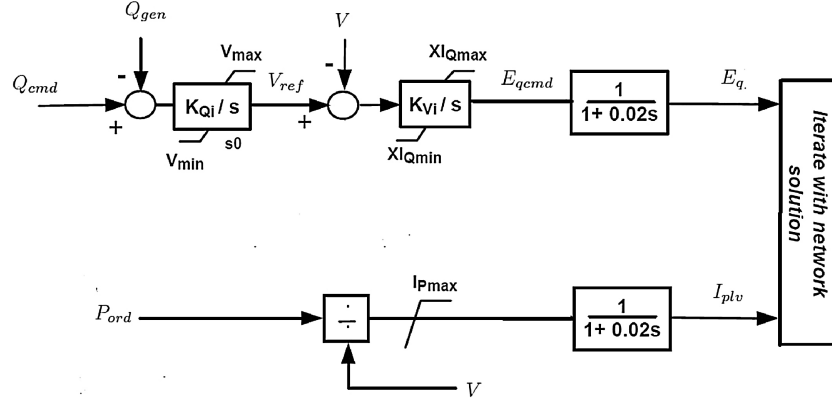


Fig. 11. Block diagram of the electrical and generator variables.

Group 5: Reactive power control (power factor case) and electrical control.

$$\frac{dP_{1elec}}{dt} = \frac{1}{T_{pwr}} [P_{elec} - P_{1elec}]. \quad (10)$$

$$\frac{dV_{ref}}{dt} = K_{Qi} [Q_{cmd} - Q_{gen}] \quad (11)$$

where

$$Q_{gen} = \frac{V(E_q - V)}{X_{eq}},$$

and

$$Q_{cmd} = \begin{cases} P_{1elec} \cdot \tan(\text{PFA}_{ref}) & \text{Power factor case} \\ Q_{ord} & \text{Supervisory voltage case} \\ \text{from another model or constant.} & \end{cases}$$

Group 6: Reactive power control (supervisory voltage case) and electrical control.

$$\frac{dQ_{droop}}{dt} = \frac{1}{T_{lpqd}} [Q_{inpt} - Q_{droop}]. \quad (12)$$

$$\frac{dV_{1reg}}{dt} = \frac{1}{T_r} [V_{reg} - V_{1reg}]. \quad (13)$$

$$\frac{dQ_{wvl}}{dt} = \frac{1}{T_v} [K_{pv}(V_{ref} - V_{1reg} - V_{qd}) - Q_{wvl}]. \quad (14)$$

$$\frac{dQ_{wvu}}{dt} = K_{iv}(V_{ref} - V_{1reg} - V_{qd}). \quad (15)$$

$$\frac{dQ_{ord}}{dt} = \frac{1}{T_c} (Q_{wvl} + Q_{wvu} - Q_{ord}). \quad (16)$$

Eq. (11) still holds in this group as well.

Group 7: Active power control and inertia control.

$$\frac{dP_{avf}}{dt} = \frac{1}{T_{pav}} [P_{avf} - P_{avf}]. \quad (17)$$

$$\frac{d(\text{fltdfwi})}{dt} = \frac{1}{T_{ipwi}} [\text{dfdbwi} - \text{fltdfwi}]. \quad (18)$$

$$\frac{d(\text{dpwi})}{dt} = \frac{K_{wi}}{T_{ipwi}} [\text{dfdbwi} - \text{fltdfwi}] - \frac{\text{dpwi}}{T_{wowi}}. \quad (19)$$

Group 8: DFIG generator/converter.

$$\frac{dE_{qcmd}}{dt} = K_{vi} [V_{ref} - V]. \quad (20)$$

$$\frac{dE_q}{dt} = \frac{1}{0.02} [E_{qcmd} - E_q]. \quad (21)$$

$$\frac{dI_{plv}}{dt} = \frac{1}{0.02} \left[ \frac{P_{ord}}{V} - I_{plv} \right]. \quad (22)$$

Group 9: The algebraic (network) equation (see [13]):

$$0 = (V^2)^2 - [2(P_{elec}R + Q_{gen}X) + E^2]V^2 + (R^2 + X^2)(P_{elec}^2 + Q_{gen}^2). \quad (23)$$

The algebraic equation (23) can be eliminated by using the unique terminal solution in Eq. (24).

$$V = f(I_{plv}, E_q; X; R; E) = \frac{-B + \sqrt{B^2 - 4AC}}{2A}, \quad (24)$$

with  $A = 1 + \frac{2X}{X_{eq}} + \frac{R^2 + X^2}{X_{eq}}$ ,  $B = -\left[2I_{plv}R + \frac{2XE_q}{X_{eq}} + \frac{2(R^2 + X^2)E_q}{X_{eq}}\right]$ , and

$C = \frac{R^2 + X^2}{X_{eq}} + (R^2 + X^2)I_{plv}^2 - E^2$ . The elimination of the algebraic constraint proof is given in the Appendix. Tables 1–3 show the parameters and control limits (see [5,13,15]).

Remark: The system size can be reduced based on the range of wind speeds (see section 2.C in [15] or [22] for greater details). Also, we ran a Simulink verification to test the similarity between the differential equations introduced in this section (solved by ODE15s in Matlab) and the block diagrams in transfer function. The results were typical.

### 2.3. Comparison and validation with real data

**Validation vs. industry documentation:** The proposed model matches GE documentation in [5], pp. 34–35, in two major information. First, our model shows that the pitch angle  $\theta$  has to be about  $26^\circ$  when  $v_{wind} = 25$  m/s (see Fig. 6). These numbers matches what is documented in [5] that the maximum allowable  $v_{wind}$  is about 25 m/s and that the pitch cannot have an angle more than  $26^\circ$ . Second,  $w_{ref}$  reaches the rated value (1.2 pu) at  $P_{elec} \approx 0.45$  pu in our model (see

**Table 1**  
Summary of control limits to be applied as in [5].

Variable	Lower bound	Higher bound
$Q_{wvu} + Q_{wvl}$	$Q_{min} = -0.436$	$Q_{max} = 0.436$
$V_{ref}$	$V_{min} = 0.9$	$V_{max} = 1.1$
$E_{qcmd}$	$Xl_{Qmin} = 0.5$	$Xl_{Qmax} = 1.45$
$\frac{I_{plv}}{V}$	0	$I_{pmax} = 1.1$
$\theta$	$\theta_{min} = 0$	$\theta_{max} = 27$
$P_{inp}$	$P_{wmin} = 0.04$	$P_{wmax} = 1.12$
$\frac{dP_{inp}}{dt}$	$dP_{min} = -0.45$	$dP_{max} = 0.45$
$\frac{d\theta}{dt}$	$d\theta = -10$	$d\theta = 10$

**Table 2**  
Parameter used in the model are Per Unit (pu).

Parameter	Value
$w_0$	1 (any choice bigger than 0)
$D_{ig}$	1.5 (60 Hz) or 2.3 (50 Hz)
$K_{ig}$	1.11 (60 Hz, 1.5 MW)
$K_{ig}$	1.39 (50 Hz, 1.5 MW)
$\frac{1}{2}\rho A_r, K_b$	0.00159 and 56.6 respectively
$w_{base}$	125.66 (60 Hz) or 157.08 (50 Hz)
$H(\text{two mass})$	4.33
$H(\text{one mass})$	4.94 (60 Hz), 5.29 (50 Hz)
$H_g$	0.62 (60 Hz), 0.96 (50 Hz)
$K_{pp}, K_{ip}$	150, 25 respectively
$K_{pc}, K_{ic}$	3, 30 respectively
$T_p, p_{stl}$	0.3, 1 respectively
$T_{pc}, K_{pprq}$	0.05, 3 respectively
$K_{itrq}, T_w$	0.6, 1 respectively
$T_{pwr}, K_{Qi}$	0.05, 0.1 respectively
$T_{lqds}, T_r$	5, 0.02 respectively
$T_v, K_{pv}$	0.05, 18 respectively
$K_{iv}, T_c$	5, 0.15 respectively
$T_{pav}, T_{ipwi}$	0.15, 1 respectively
$K_{wb}, T_{wowi}$	10, 5.5 respectively
$K_{vb}, X_{eq}$	40, 0.8 respectively
$R, E$	0.02, 1.0164 respectively
$X = X_l + X_r$	$X_l = 0.0243, X_r = 0.00557$ respectively

**Table 3**  
 $C_p$  coefficients  $\alpha_{i,j}$ .

$i$	$j$	$\alpha_{i,j}$	$i$	$j$	$\alpha_{i,j}$
4	4	4.9686e-10	4	3	-7.1535e-8
4	2	1.6167e-6	4	1	-9.4839e-6
4	0	1.4787e-5	3	4	-8.9194e-8
3	3	5.9924e-6	3	2	-1.0479e-4
3	1	5.7051e-4	3	0	-8.6018e-4
2	4	2.7937e-6	2	3	-1.4855e-4
2	2	2.1495e-3	2	1	-1.0996e-2
2	0	1.5727e-2	-	-	-
1	4	-2.3895e-5	1	3	1.0683e-3
1	2	-1.3934e-2	1	1	6.0405e-2
1	0	-6.7606e-2	0	4	1.1524e-5
0	3	-1.3365e-4	0	2	-1.2406e-2
0	1	2.1808e-1	0	0	-4.1909e-1

Figs. 4 and 12), which also matches the documented information in GE reports. Notice that since  $w_{ref}$  dynamics match the correct information, the shaft speed also will.

**Comparison and validation with real data:** In order to compare the proposed model with another one, we need to select a model that includes most of the WTG's control blocks similar to how our model is. The model proposed and studied by [13] mainly cited [8], both of

which are highly cited from scholars working on WTGs studies. Therefore, we will focus on one of the differences between the proposed model and the models [13,8]. Our focus for comparison will be on  $w_{ref}$  control. Both the generator and turbine speeds are controlled by the reference speed  $w_{ref}$  (see Rotor Model explanation in Section 2.1). The proposed model and [13,8] have  $w_{ref}$  following a different curve for lower wind speeds ( $w_{ref} = -0.67P_{elec}^2 + 1.42P_{elec} + 0.51$ ) as opposed to the proposed model ( $w_{ref} = -0.75P_{elec}^2 + 1.59P_{elec} + 0.63$ ). Fig. 12 shows the curves  $w_{ref}$  our model and [13] follow until the rated value 1.2 pu. To test the effects of this difference on the WTG, we simulated the power-wind speed profile (stable steady state of  $P_{elec}$  vs.  $v_{wind}$ ) from our model and [13] and plotted them vs. real measured data over hours in the day (see the Acknowledgment for more information about the data providers). Fig. 13 shows this validation and comparison with real measure data. In Fig. 12 we see that  $w_{ref}$  reaches the rated value (1.2 pu) at  $P_{elec} \approx 0.45$  pu in our model, while it reaches the rated value (1.2 pu) at  $P_{elec} \approx 0.75$  pu in their model [13]. This means that our dynamics for both the reference and the shaft speeds, are by far, more accurate in reflecting the manufacturer's documentation, as explained earlier in this subsection. The power-wind speed profile results from our model is better than [13,8] when compared to the real time measured data (Fig. 13). The stable steady state of  $P_{elec}$  does not have to average the dynamic measured data, but for large numbers of measured data (the case in our trial) we expect the data to be close to some form of normal distribution around the stable steady state. Our model shows better results in that sense.

### 3. The effect of the Q Droop function on the WTG dynamics

By considering the system in the supervisory mode and two mass rotor model, the model of differential equations reduces to Eqs. (1)–(7), (11)–(16), and (20)–(22). The system can be reduced again based on the wind speed range of interest as clarified in [16], section 2.C.

#### 3.1. The system without Q Droop

The WTG system works with either the reactive power in power factor set up (Group 5 in section 2.B) or with the reactive power in supervisory voltage set up (Group 6 in section 2.B). If the system is in power factor case, then there is no  $Q_{droop}$  function element present, and no stability issue exists as discussed in [15,16]. Since the supervisory voltage mode is associated with the WTG being a unit in a compound of WTGs, it is important to study how the reactive power control and the system behaves with and without the Q Droop. In order to achieve that we exclude  $Q_{droop}$  from the dynamics by setting  $V_{qd} = 0$  (see Fig. 9) and therefore Eq. (12) is eliminated. We computed the eigenvalues at the steady state, see Table 4.

As Table 4 shows, the eigenvalue  $\lambda_{14}$  has a real positive part (+0.32). This shows that the system is not resilient against even local

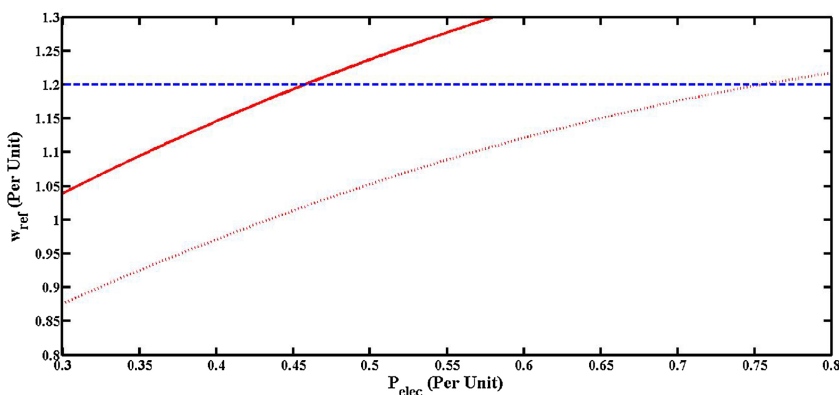


**Fig. 12.**  $w_{ref}$  from the proposed model (solid) vs. [13,8] (dotted) and the rated speed (dashed).

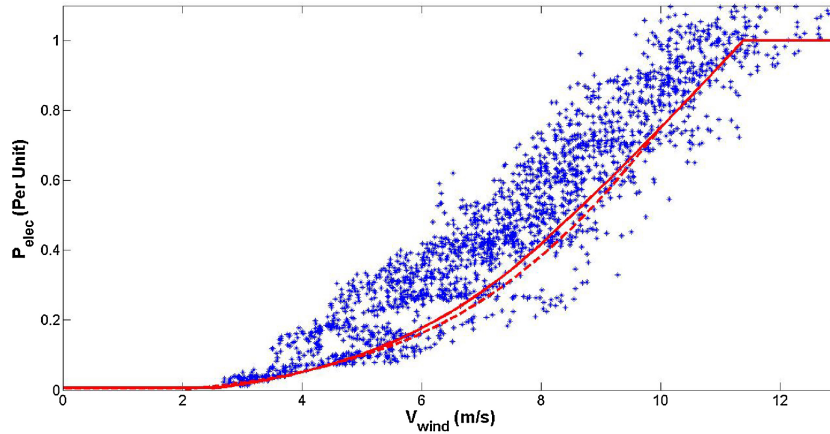


Fig. 13. Real data of a WTG (stars) vs. power-wind speed curves for the proposed model (solid) and [13,8] (dashed).

**Table 4**  
Eigenvalues of the steady states without Q Droop. Real of  $\lambda_{14}$  (cause of instability) is bold.

	Real	Imag
$\lambda_1$	-52.25	0
$\lambda_2$	-48.94	0
$\lambda_3$	-19	0
$\lambda_4$	-16.15	0
$\lambda_{5,6}$	-1.35	$\pm 11.87$
$\lambda_7$	-8.84	0
$\lambda_{8,9}$	-1.28	$\pm 2.15$
$\lambda_{10,11}$	-0.25	$\pm 1.31$
$\lambda_{12}$	-1	0
$\lambda_{13}$	-0.16	0
$\lambda_{14}$	<b>+0.32</b>	0
$\lambda_{15}$	-50	0

disturbances and is always in need of limiters. We computed the eigenvector that corresponds to  $\lambda_{14}$  to see the state variables that are locally affected by the instability. As shown in Table 5, the normalized eigenvector components have weights not only on the directions of the integrators  $Q_{wvl}$  and  $Q_{wvu}$ , but also on the directions of  $Q_{ord}$ ,  $V_{ref}$ ,  $E_{qcmd}$ ,  $E_q$ , and  $I_{plv}$ .

3.2. Q Droop as a constant

Based on our trials, if we consider  $Q_{droop}$  as a constant, it provides a reduction to the effective reference voltage. However, if  $V_{reg}$  is a constant as well, we found the system still unstable. Table 6 shows some of the state variables computed vs.  $Q_{droop} = constant$ . Table 6 shows that  $Q_{droop}$  should be a very small value. As noticed  $Q_{droop} > 0.03$  results in extreme values of the steady states that are completely unrealistic and out of the control limits mentioned in Table 1.

3.3. Q Droop with  $Q_{gen}$  as input vs. different gains

In the case of  $11.4 < V_{wind} < 25$ , the pitch control forces the physical state variables to be constant, as the rated power is achieved at  $V_{wind} = 11.4$  m/s. In order to do this, the pitch angle changes from 0 to 26, as in Fig. 6, while Table 7 shows the steady state values. We used the value of  $K_{qd} = 0.04$  as suggested in [5]. We tried a variation of the

**Table 5**  
Eigenvector that corresponds to  $\lambda_{14}$  by components.

Variable	$f_1, w_g, w_t, \Delta\theta_m, P_{imp}$	$Q_{ord}$	$V_{ref}$	$E_{qcmd}$	$E_q$	$I_{plv}$	$Q_{wvl}$	$Q_{wvu}$
Component	$\approx 0$	0.62	0.01	0.44	0.44	-0.01	0.34	0.3

**Table 6**  
Physical steady states vs.  $Q_{droop}$  in constant case.

State variable	$w_g$	$V$	$Q_{gen}$	$E_q$	$I_{plv}$
$Q_{droop} = 0.01$	0.2	1.026	-0.3	0.78	0.97
$Q_{droop} = 0.02$	0.2	1.036	0.037	1.06	0.96
$Q_{droop} = 0.03$	0.2	1.046	0.38	1.34	0.95
$Q_{droop} = 0.04$	0.2	1.056	0.74	1.62	0.94
$Q_{droop} = 0.05$	0.2	1.066	1.11	1.9	0.93
$Q_{droop} = 0.06$	0.2	1.076	1.49	2.18	0.92

**Table 7**  
Physical steady states for  $11.4 < V_{wind} < 25$  m/s.

State variable	$w_g$	$V$	$Q_{gen}$	$E_q$	$I_{plv}$
Value	0.2	1.03	-0.154	0.911	0.97

**Table 8**  
Physical steady states vs. the parameter  $K_{td}$ .

State variable	$w_g$	$V$	$Q_{gen}$	$E_q$	$I_{plv}$
$K_{td} = 0.02$	0.2	1.04	0.19	1.19	0.96
$K_{td} = 0.03$	0.2	1.019	-0.58	0.59	0.98
$K_{td} = 0.04$	0.2	1.03	-0.154	0.911	0.97
$K_{td} = 0.05$	0.2	1.032	-0.08	0.97	0.96
$K_{td} = 0.06$	0.2	1.033	-0.05	0.99	0.96

gain  $K_{td}$  with a fixed  $v_{wind} = 11.4$  m/s and computed the steady states in Table 8 and the eigenvalues in Table 9. We noticed a change of  $K_{td}$  from 0.04 to 0.06 (50% change) resulting in 67%, 0.3%, 8.6%, and 1% in  $Q_{gen}$ ,  $V$ ,  $E_q$ ,  $I_{plv}$  respectively, while some of the eigenvalues exceeded a 100% change. In Table 9, the last column shows the change in percentage for the real and imaginary parts respectively. The gain  $K_{dq}$  affects both the steady states and their trajectories' behaviors (because of the eigenvalues sensitivity to  $K_{dq}$ ), so a parameter estimate study for  $K_{dq}$  should be conducted based on the application conditions.

**Table 9**  
Eigenvalues of the steady states at  $v_{wind} = 11.4$  m/s.

	Real $K_{td}=0.04$	Imag $K_{td}=0.04$	Real $K_{td}=0.06$	Imag $K_{td}=0.06$	% change
$\lambda_1$	-52.25	0	-52.25	0	0, 0
$\lambda_2$	-48.94	0	-48.94	0	0, 0
$\lambda_3$	-19	0	-19	0	0, 0
$\lambda_4$	-16.11	0	-16.11	0	0, 0
$\lambda_{5,6}$	-1.34	$\pm 12.15$	-1.35	$\pm 12.15$	0.74, 0
$\lambda_7$	-3.14	0	-3.14	0	0, 0
$\lambda_{8,9}$	-0.1	$\pm -1.19$	-0.002	$\pm 1.18$	98, 0.84
$\lambda_{10,11}$	-0.18	$\pm 0.46$	-0.18	$\pm 0.46$	0, 0
$\lambda_{12}$	-0.13	0	-0.13	0	0, 0
$\lambda_{13}$	-8.83	0	-8.82	0	0.11, 0
$\lambda_7$	-3.14	0	-3.14	0	0, 0
$\lambda_{15,16}$	-0.096	$\pm 0.14$	-0.2	$\pm 0.21$	108, 50

3.4. Simulation of Q Droop function effect in stabilizing the system after sudden changes

By running a simulation for a pulse wind speed profile with and without  $Q_{droop}$  function, we can see how the integrator variables  $Q_{wvl}$  and  $Q_{wvu}$  behave, as well as the whole dynamics. The same can be done for a severe drop in  $X$  passing through the Hopf bifurcation found in [16] to see if the integrators and the system will stabilize after clearing the drop. The wind profile found in Fig. 14 and severe drop-clear case of  $X$  in Fig. 15 should crystallize the point as to what this function is of great importance to the reactive power control as claimed in [5]. In Fig. 14, the integrators seem unable to converge again to the previous

**Table 10**  
Summary of the simulation trials to test attraction limits vs. control limits.

	Trial: initial condition exceeds control limits	Trial: sudden change in $v_{wind}$	Trial: drop-clear in $V$	Trial: severe drop in $X$
Case 1	Fig. 16	Fig. 18	Fig. 20	Fig. 22
Case 2	Fig. 17	Fig. 19	Fig. 21	Fig. 23

steady state before the pulse occurred. Once the pulse wind passed without the  $Q_{droop}$ , the system diverged. In real life the control limits will prevent such divergences and the system will settle down once more after the effect of the wind pulse has passed. However, the same pulse effect could not force the integrators to diverge under the effect of the  $Q_{droop}$  function. This implies that the use of this function helps in stabilizing the system by improving the integrator functions which is of great practical benefit for addressing disturbances due to wind speed. In Fig. 15, the system using the  $Q_{droop}$  function shows resilience to the severe drop in  $X$ . The integrators did not diverge and proceeded to settled down after the drop was cleared, unlike the case when we did not use the  $Q_{droop}$  for which the system remained unstable after the drop was cleared.

3.5. Summary of stability issues found with and without the Q Droop

- 1) The model in supervisory voltage case without the Q Droop function: In this case, the model does not have local stability and is not resilient against local disturbances.
- 2) The model in supervisory voltage case with the Q Droop function: If

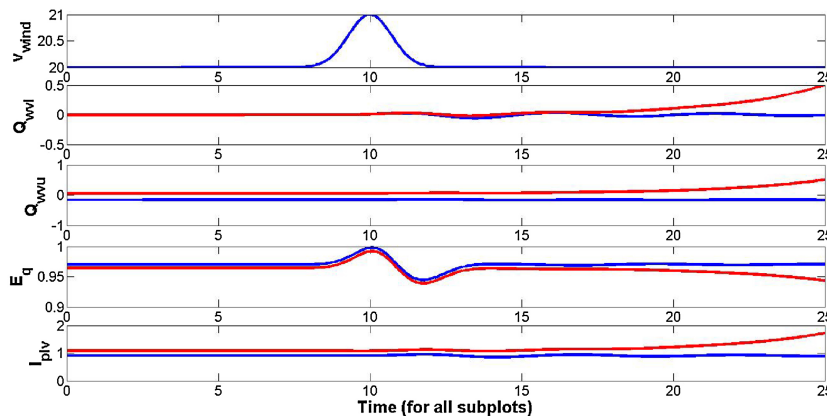


Fig. 14. System response with  $Q_{droop}$  function (blue) and without it (red) for a pulse wind profile. (For interpretation of the references to color in this figure legend, the reader is referred to the web version of the article.)

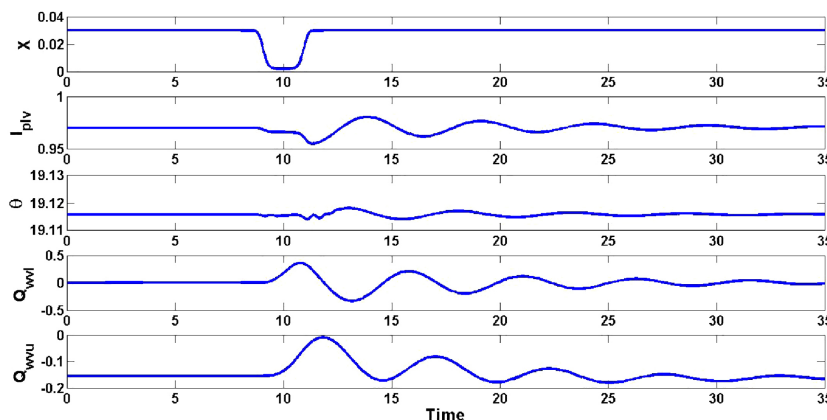


Fig. 15. System response with  $Q_{droop}$  function for a severe drop in the reactance  $X$  passing through Hopf bifurcation.

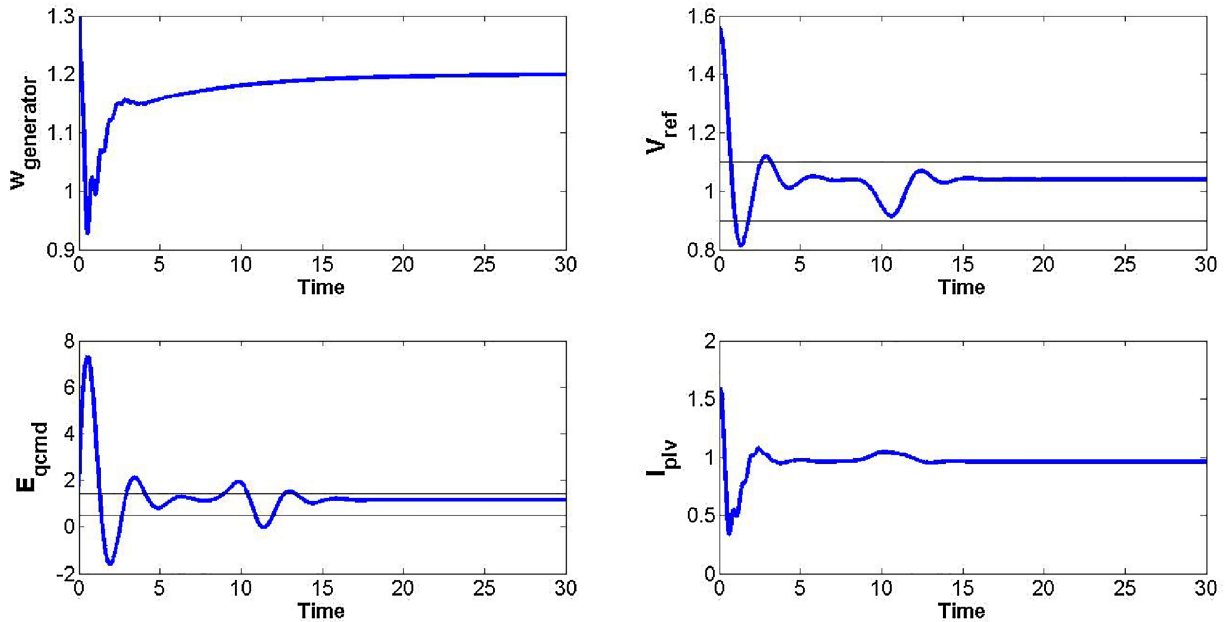


Fig. 16. Case 1: system response (blue) to initial condition exceeds control limits (black). (For interpretation of the references to color in this figure legend, the reader is referred to the web version of the article.)

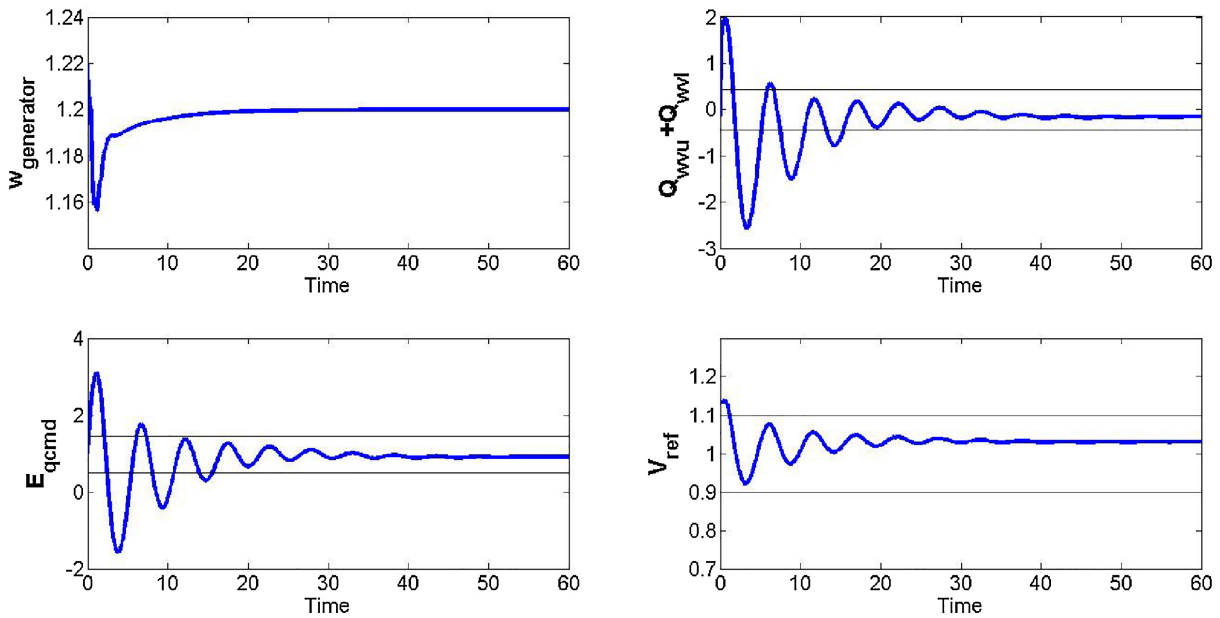


Fig. 17. Case 2: system response (blue) to initial condition exceeds control limits (black). (For interpretation of the references to color in this figure legend, the reader is referred to the web version of the article.)

the Q Droop function is just a constant, the system is still unstable. Though applying the constant Q Droop function reduces the effect of increasing reference voltage during the dynamics.

- 3) The model in supervisory voltage case with the Q Droop function as a proportion feedback of  $Q_{gen}$ : This case guarantees local stability and stabilizes the whole system. This conclusion is based on the eigenvalue analysis done in section 3.C and with different values for the gain  $K_{td}$ .

#### 4. Attraction limits vs. control limits

To the best of our knowledge, there have never been a study for the attraction limits vs. control limits (Table 1). The WTG system is stable

in the power factor case, as well as the supervisory mode when the Q Droop function has a feedback from  $Q_{gen}$  (as discussed in previous section), so these are the cases where we study attraction limits. We summarize our numerical trials to test the interaction between the attraction limits vs. the control limits in Table 10. We refer to the power factor case as “case 1” and the Q Droop function in feedback mode as “case 2”. Below is the reason for and objective of our trials:

- 1) We ran simulations for the dynamics as initial conditions exceed the control limits, so we checked directly if the attraction limits were larger than the control limits.
- 2) The control limits, as shown in Table 1, include limits on  $\frac{dP_{inp}}{dt}$  and  $\frac{d\theta}{dt}$

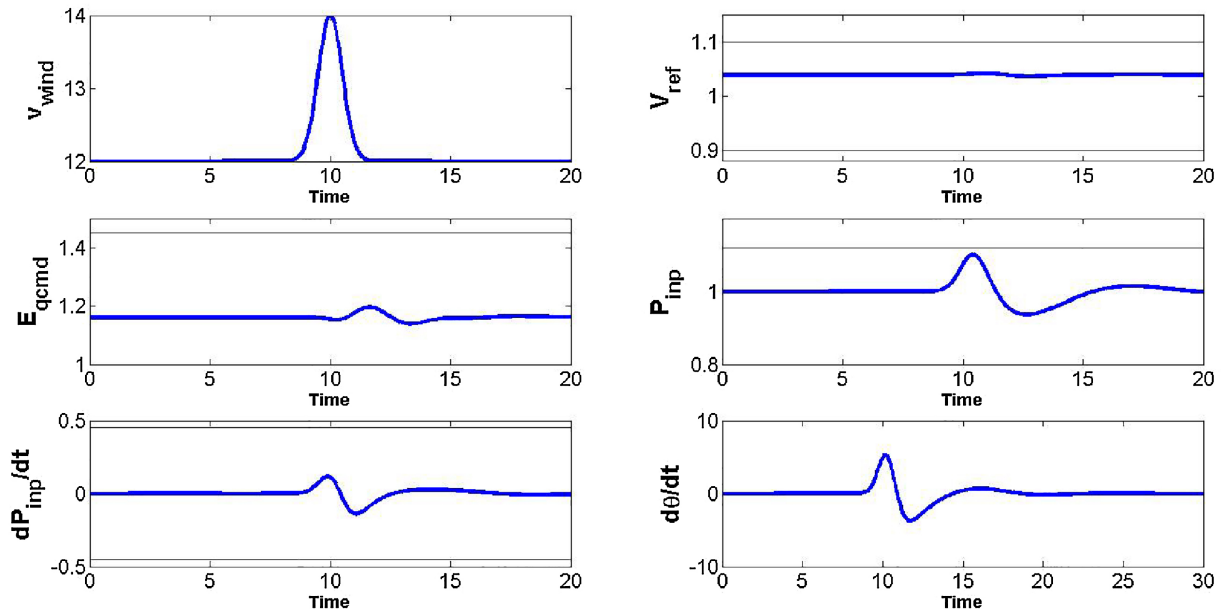


Fig. 18. Case 1: system response (blue) vs. control limits (black) for a given  $v_{wind}$  profile. (For interpretation of the references to color in this figure legend, the reader is referred to the web version of the article.)

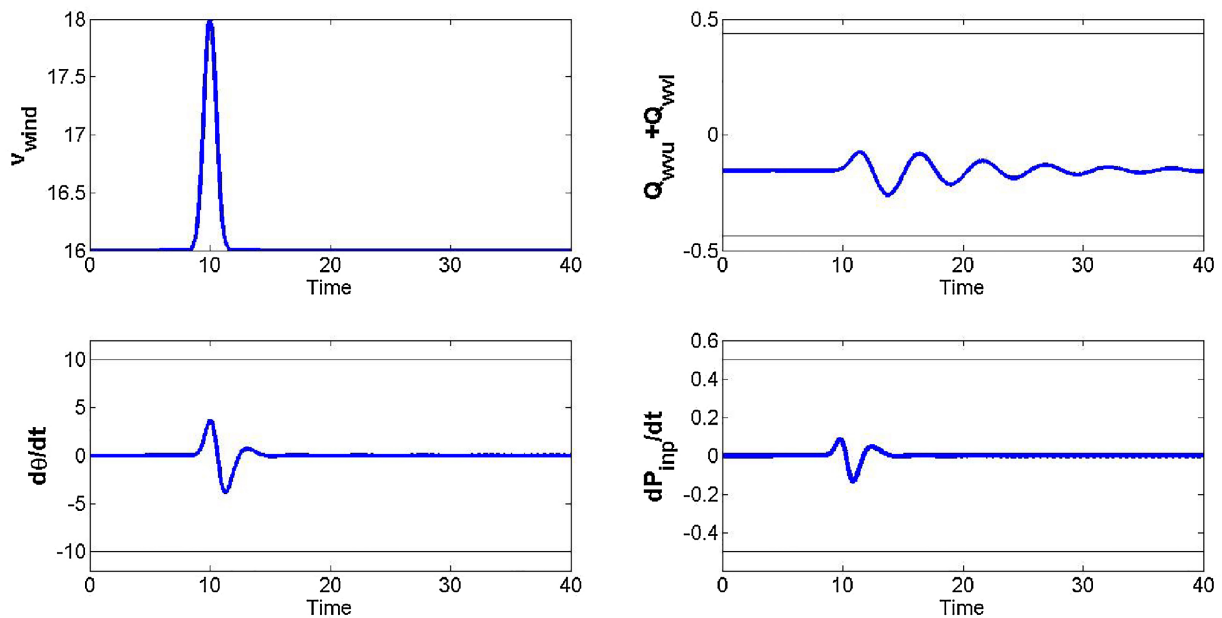


Fig. 19. Case 2: system response (blue) vs. control limits (black) for a given  $v_{wind}$  profile. (For interpretation of the references to color in this figure legend, the reader is referred to the web version of the article.)

that are mostly for mechanical constrains. Therefore, we should test these derivatives, especially when there is a sudden change in  $v_{wind}$  ( $\theta$  and  $P_{inp}$  are sensitive to  $v_{wind}$  as concluded in [15]).

- 3) A severe drop in  $X$  passing through the Hopf bifurcation found in [16] seems to test the system's resilience and it is an extreme case that can capture the interactions between the attraction limits vs. control limits. We can do a similar test if we have a drop in  $V$  as well.
- 4) In all the simulations for case 2, we present the sum of the integrators  $Q_{wvu}$  and  $Q_{wvl}$  vs. the limit imposed on them, as this is one of the major practical applications for the Q Droop function (claimed by GE [5]).

From the trials we can observe the following:

- 1) The attraction limits do exceed the control limits.
- 2) In all extreme cases (sudden wind change, drop in  $V$ , and severe drop in  $X$ ) the system seems resilient. The trajectories were bounded under the control limits, except with the drop in  $V$ . However, even in that case, trajectories settled down again and returned to within the control limits.
- 3) The limits for both  $\frac{dP_{inp}}{dt}$  and  $\frac{d\theta}{dt}$  seem safe and reasonable, as the derivatives did not exceed the limits even in the extreme cases.
- 4) The Q Droop function strongly stabilizes the system and controls the behavior of the integrators as they have been under the limits even in the extreme cases.
- 5) A great benefit from these results is to allow scholars to run simulations for the system without the challenge of imposing the control limits, especially for small-signal stability purposes.

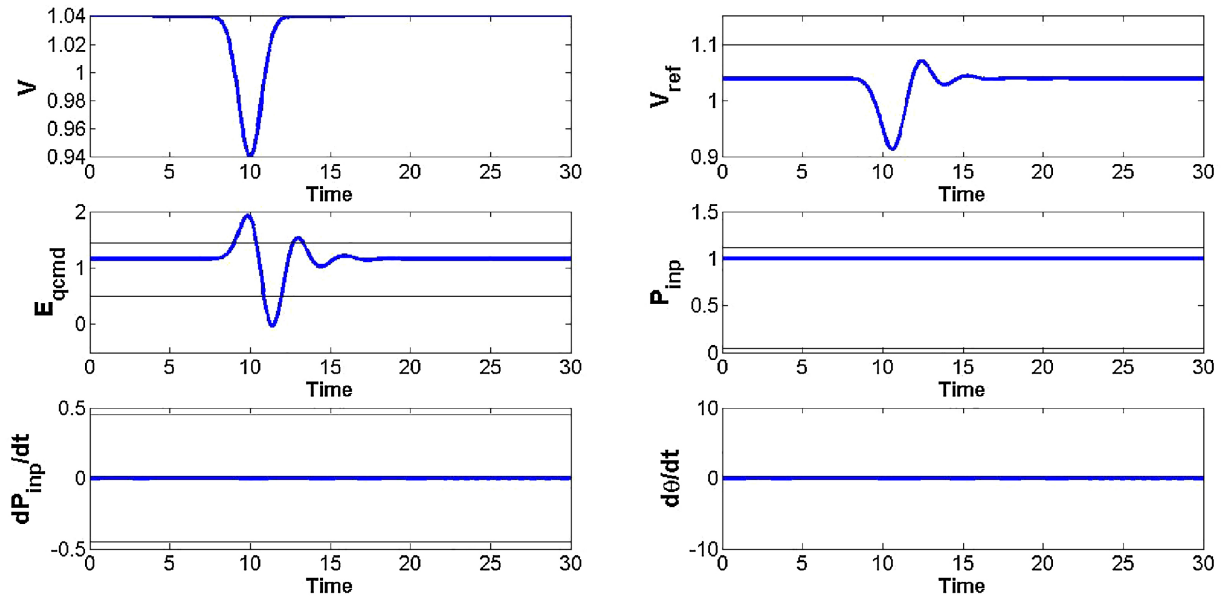


Fig. 20. Case 1: system response (blue) vs. control limits (black) for a drop in  $V$ . (For interpretation of the references to color in this figure legend, the reader is referred to the web version of the article.)

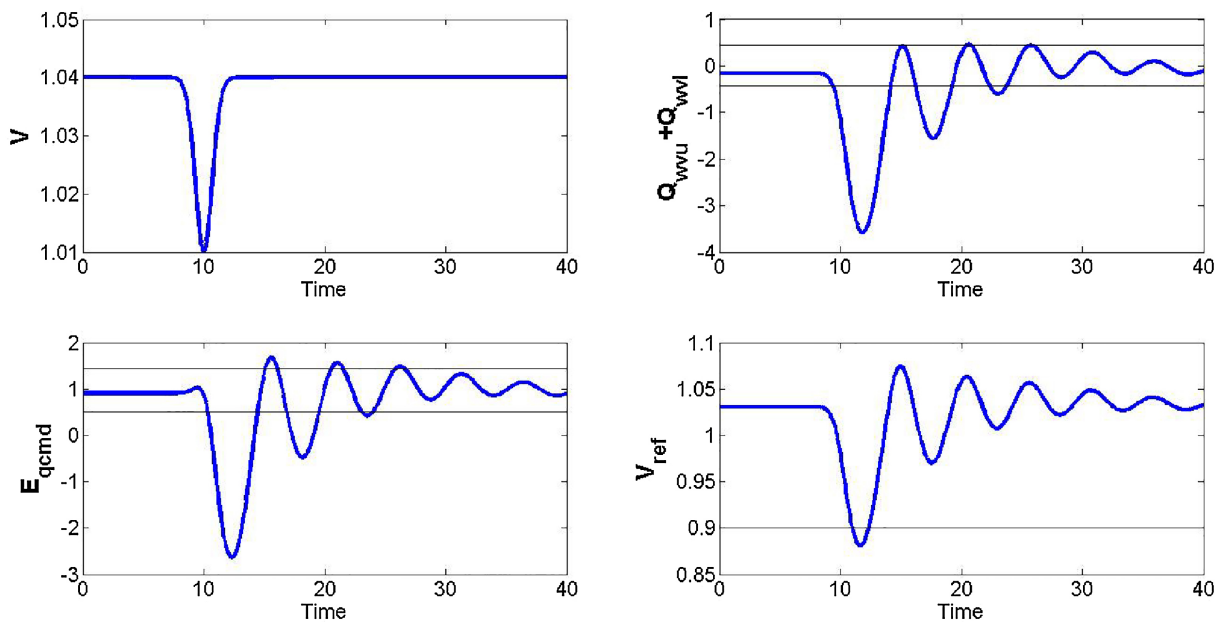


Fig. 21. Case 2: system response (blue) vs. control limits (black) for a drop in  $V$ . (For interpretation of the references to color in this figure legend, the reader is referred to the web version of the article.)

### 5. Conclusion, significance of the results and recommendations

**Modeling of WTGs:** This paper introduced an inclusive mathematically formulated model to present WTGs dynamics. The model has been explained block by block in terms of their functions, their variables, parameters and representative differential equations in Section 2. Moreover, the proposed model has been validated vs. manufacturer's documentation along with real measured data.

**Q Droop analysis and practical significance:** The Q Droop function has been defined for all cases (constant and feedback), mathematically formulated, and tested by simulations in extreme scenarios in Section 3. The paper explained and further investigated the Q Droop function's effect on the integrators in the reactive power control. Moreover, the paper documented the stability in the cases when the Q

Droop is just a constant (not recommended) and the effect of the gain parameter tuning. Lastly, the paper recommends the use of the Q Droop function and confirmed that the system increases its resilience by having it in the feedback mode. Also, the paper recommends careful study of the gain parameter associated with the Q Droop as the dynamics show sensitivity toward it.

**Control limits:** The control limits (limiters) suggested by many in literature to be placed on the system, has been challenged and investigated, for the first time in literature. Our study and tests show that the limiters are included in many cases inside the attraction limits for the stable steady states. Furthermore, for extreme changes and scenarios, the limiters associated with some derivatives, seem to be with no, or minimal, practical significance. Given that our model is an extension for the GE [4,5] models, where these limiters were introduced,

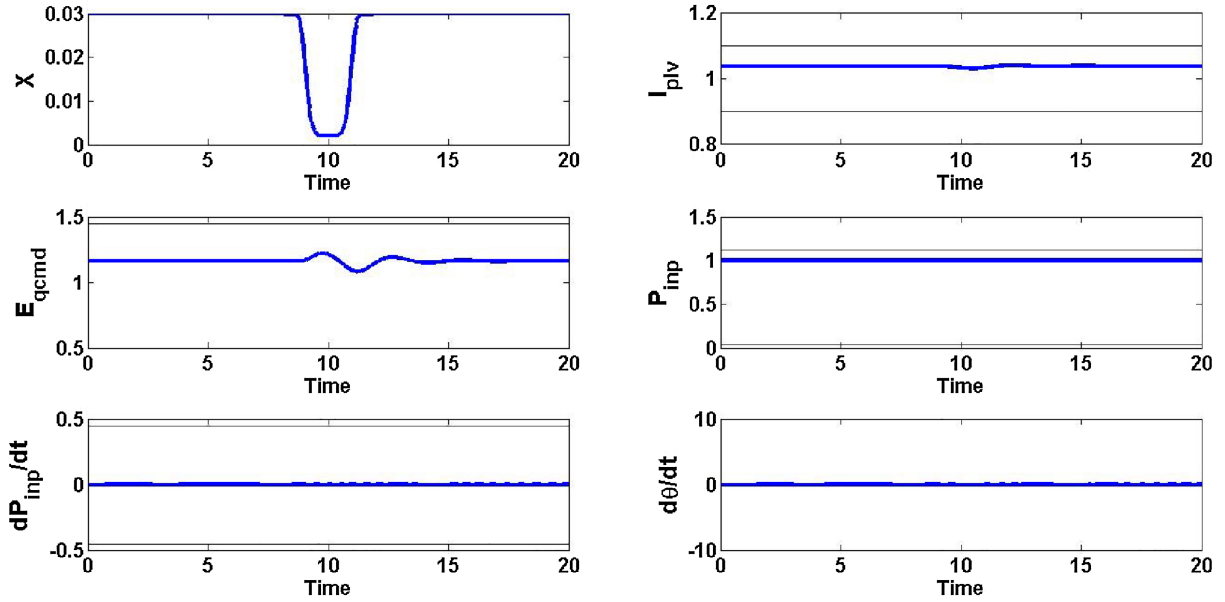


Fig. 22. Case 1: system response (blue) vs. control limits (black) for a drop in  $X$  passing through a Hopf bifurcation. (For interpretation of the references to color in this figure legend, the reader is referred to the web version of the article.)

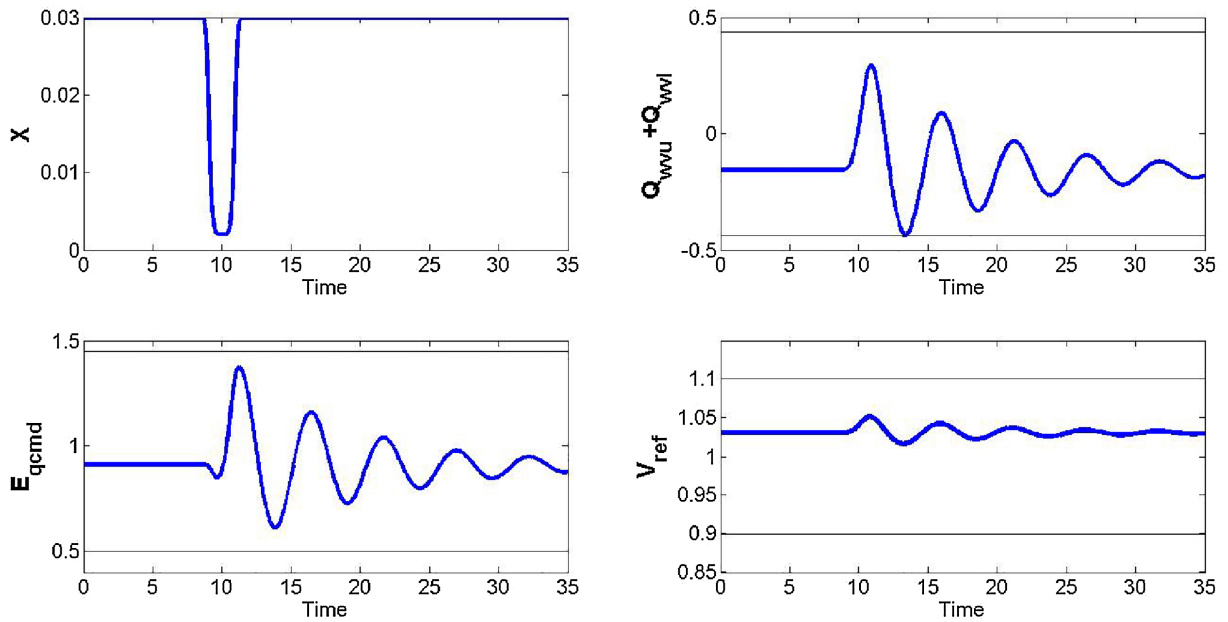


Fig. 23. Case 2: system response (blue) vs. control limits (black) for a severe drop in  $X$ . (For interpretation of the references to color in this figure legend, the reader is referred to the web version of the article.)

it is important to further study this phenomenon and if the limiters need to be removed/relaxed or the modeling need to improve.

### Acknowledgments

The author of the paper would like to thank the North American Wind Research and Training Center for sharing data with Dr. Kevin

### Appendix A

**Lemma 1.** In the steady state, if  $E_q$ ,  $E_{qcmd}$  and  $I_{plv}$  are bounded by the limits given in Table 1, such that  $0.5 \leq E_q = E_{qcmd} \leq 1.45$ ,  $I_{plv} = \frac{P_{ord}}{V} \leq 1.1$  ( $E_q$ ,  $E_{qcmd}$ ,  $I_{plv}$ ), and the  $V$  is real, then there exists a unique solution for Eq. (23) such that the possible scenario  $V > E = 1.0164$  can possibly happen.

**Proof.** By setting  $Q_{gen} = \frac{V(E_q - V)}{X_{eq}}$  (see Eq. (11)) and  $P_{elec} = I_{plv}V$  (see Eq. (3)), Eq. (23) becomes,

Wedeward, Dean of Engineering at New Mexico Tech, who first introduced the data with the author of this paper in their previous work [25]. This same data has been used in Section 2 of this paper (Fig. 13). For more information about the data used, please see: <http://www.mesalands.edu/news-releases/the-north-american-wind-research-and-training-center-shares-data-with-new-mexico-tech-to-enhance-the-future-research-of-wind-energy-technology/>.

$$0 = V^4 - 2(I_{plv}V)RV^2 - 2 \cdot \frac{V(E_q - V)}{X_{eq}} \cdot XV^2 - E^2V^2 + (R^2 + X^2)I_{plv}^2V^2 + (R^2 + X^2) \cdot \frac{V^2(E_q - V)^2}{X_{eq}}. \quad (25)$$

Dividing by  $V^2$  and algebraic re-arrangement gives,

$$0 = V^2 \left[ 1 + \frac{2X}{X_{eq}} + \frac{R^2 + X^2}{X_{eq}} \right] - V \left[ 2I_{plv}R + \frac{2XE_q}{X_{eq}} + \frac{2(R^2 + X^2) \cdot E_q}{X_{eq}} \right] + \left[ \frac{R^2 + X^2}{X_{eq}} + (R^2 + X^2) \cdot I_{plv}^2 - E^2 \right]. \quad (26)$$

With  $A = 1 + \frac{2X}{X_{eq}} + \frac{R^2 + X^2}{X_{eq}}$ ,  $B = - \left[ 2I_{plv}R + \frac{2XE_q}{X_{eq}} + \frac{2(R^2 + X^2)E_q}{X_{eq}} \right]$ , and  $C = \frac{R^2 + X^2}{X_{eq}} + (R^2 + X^2)I_{plv}^2 - E^2$ , then:

$$V = \frac{-B \pm \sqrt{B^2 - 4AC}}{2A}. \quad (27)$$

With  $R, X, X_{eq} > 0$ , we have  $A > 0$ . If we use the parameter values of  $R, X$ , and  $X_{eq}$  given in Table 2 and the upper bounds given in Lemma 1, we get:

$$\frac{-B}{2A} = \frac{2I_{plv}R + \frac{2XE_q}{X_{eq}} + \frac{2(R^2 + X^2) \cdot E_q}{X_{eq}}}{2 \left( 1 + \frac{2X}{X_{eq}} + \frac{R^2 + X^2}{X_{eq}} \right)} < 0.99. \quad (28)$$

This implies that there exists a unique solution for  $V$  such that  $V > 1.0164$  and that solution is:

$$V = f(I_{plv}, E_q; X; R; E) = \frac{-B + \sqrt{B^2 - 4AC}}{2A} \quad (29)$$

with  $A, B$ , and  $C$  from Eq. (26).

## References

- [1] Department of Energy, Energy Dept. Reports: U.S. Wind Energy Production and Manufacturing Reaches Record Highs, (2013) (accessed 25.09.15), <http://energy.gov/articles/energy-dept-reports-us-wind-energy-production-and-manufacturing-reaches-record-highs>.
- [2] S. Heier, *Grid Integration of Wind Energy Conversion Systems*, 2nd edition, John Wiley & Sons, 2006.
- [3] A. Tummala, R.K. Velamati, D.K. Sinha, V. Indrāja, V.H. Krishna, A review on small scale wind turbines, *Renew. Sustain. Energy Rev.* 56 (2016) 1351–1371.
- [4] N.W. Miller, W.W. Price, J.J. Sanchez-Gasca, Dynamic modeling of GE 1.5 and 3.6 wind turbine-generators, Report, General Electric International, Inc., October 2003.
- [5] K. Clark, N.W. Miller, J.J. Sanchez-Gasca, Modeling of GE wind turbine-generators for grid studies, Report, General Electric International, Inc., April 2010.
- [6] P. Pourbeik, Specification of the second generation generic models for wind turbine generators, Report, Electric Power Research Institute, January 2014.
- [7] J.G. Sloomweg, H. Polinder, W.L. Kling, General model for representing variable speed wind turbines in power system dynamics simulations, *IEEE Trans. Power Syst.* 18 (1) (2003) 144–151.
- [8] W.G. C4.601, Modeling and dynamic behavior of wind generation as it relates to power system control and dynamic performance, Report, CIGRE TB 328, (August 2007).
- [9] B. Novakovic, Y. Duan, M. Solveson, A. Nasiri, D.M. Ionel, Comprehensive modeling of turbine systems from wind to electric grid, 2013 IEEE Energy Conversion Congress and Exposition (2013).
- [10] G. Ofualagba, E.U. Ubeku, Wind energy conversion system-wind turbine modeling, 2008 IEEE Power and Energy Society General Meeting – Conversion and Delivery of Electrical Energy in the 21st Century (2008).
- [11] J. He, Q. Li, S. Qin, R. Wang, DFIG wind turbine modeling and validation for LVRT behavior, 2012 IEEE Innovative Smart Grid Technologies – Asia, ISGT Asia 2012 (2012).
- [12] X. Jin, L. Li, W. Ju, Z. Zhang, X. Yang, Multibody modeling of varying complexity for dynamic analysis of large-scale wind turbines, *Renew. Energy* 90 (2016) 336–351.
- [13] G. Tsourakis, B. Nomikos, C. Vournas, Effect of wind parks with doubly fed asynchronous generators on small-signal stability, *Electr. Power Syst. Res.* 79 (1) (2009) 190–200.
- [14] J. Rose, I.A. Hiskens, Estimating wind turbine parameters and quantifying their effects on dynamic behavior, *IEEE Power and Energy Society General Meeting – Conversion and Delivery of Electrical Energy in the 21st Century* (2008).
- [15] S.A. Eisa, K. Wedeward, W. Stone, Sensitivity analysis of a type-3 DFAG wind turbine's dynamics with pitch control, 2016 IEEE Green Energy and Systems Conference (IGSEC) (2016) 1–6, <https://doi.org/10.1109/IGESC.2016.7790064>.
- [16] S.A. Eisa, W. Stone, K. Wedeward, Mathematical modeling, stability, bifurcation analysis, and simulations of a type-3 DFIG wind turbine's dynamics with pitch control, 2017 Ninth Annual IEEE Green Technologies Conference (GreenTech) (2017) 334–341, <https://doi.org/10.1109/GreenTech.2017.55>.
- [17] S.A. Eisa, K. Wedeward, W. Stone, Time domain study of a type-3 DFIG wind turbine's dynamics: Q drop function effect and attraction vs control limits analysis, 2017 Ninth Annual IEEE Green Technologies Conference (GreenTech) (2017) 350–357, <https://doi.org/10.1109/GreenTech.2017.57>.
- [18] N. Miller, J. Sanchez-Gasca, W. Price, R. Delmerico, Dynamic modeling of GE 1.5 and 3.6 MW wind turbine-generators for stability simulations, 2003 IEEE Power Engineering Society General Meeting (2003).
- [19] S.A. Eisa, Local study of wind turbines dynamics with pitch activated: trajectories sensitivity, 2017 IEEE Green Energy and Smart Systems Conference (IGESSC), IEEE, 2017, pp. 1–6.
- [20] S.A. Eisa, W. Stone, K. Wedeward, Dynamical study of a type-3 DFIG wind turbine while transitioning from rated speed to rated power, 2017 IEEE Green Energy and Smart Systems Conference (IGESSC), IEEE, 2017, pp. 1–6.
- [21] S.A. Eisa, W. Stone, K. Wedeward, Mathematical analysis of wind turbines dynamics under control limits: boundedness, existence, uniqueness, and multi time scale simulations, *Int. J. Dyn. Control* 6 (3) (2018) 929–949.
- [22] S.A. Eisa, Mathematical modeling and analysis of wind turbines dynamics (Ph.D. thesis), New Mexico Institute of Mining and Technology, 2017.
- [23] J.R. Marden, H.P. Young, L.Y. Pao, Achieving Pareto optimality through distributed learning, 2012 IEEE 51st IEEE Conference on Decision and Control (CDC) (2012) 7419–7424, <https://doi.org/10.1109/CDC.2012.6426834>.
- [24] I.A. Hiskens, Dynamics of type-3 wind turbine generator models, *IEEE Trans. Power Syst.* 27 (1) (2012) 465–474.
- [25] S.A. Eisa, K. Wedeward, W. Stone, Wind turbines control system: nonlinear modeling, simulation, two and three time scale approximations, and data validation, *Int. J. Dyn. Control* (2018) 1–23.